Research of Pattern Formation, edited by R. Takaki, pp. 265–288.

Formation and Transitions of Patterns in Thermal Convection

Osamu SANO

Department of Physics, Faculty of General Education, Tokyo University of Agriculture and Technology, Fuchu, Tokyo 183, Japan

Abstract. Experimental and theoretical studies of pattern changes in thermal convections are made under simple boundary conditions. Firstly, typical convective patterns in thin horizontal fluid layer were visualized by tracer particles and by shadowgraph method, from which formation of patterns is examined. Secondly, thermal convection in a thin torus placed vertically in a nearly uniform negative vertical temperature gradient was investigated either by flow visualization or by direct measurement of flow field using a laser Doppler anemometer. The critical Rayleigh number, the Rayleigh number dependence of the Reynolds number as well as velocity profile of a quasi-one-dimensional flow along the loop were determined. Three-dimensional cellular structures, which show periodic or nonperiodic changes both in space and time at higher Rayleigh numbers, are studied extensively. Formation and transitions of these cellular structures are successfully explained by a set of new model equations with eight variables.

1. Introduction

Thermal convection is generated by the buoyancy force due to either the heating of the lower part or cooling of the upper part of the fluid. This fluid motion is opposed by viscous frictional force, as well as diffusion of the heat so as to reduce the non-uniformity of temperature distribution. The ratio of these effect Ra = (buoyancy force)/[(thermal diffusion) (viscous force)] = $\rho\alpha\Delta T g d^3/(\kappa\mu)$ is called the Rayleigh number. Here ρ, α, κ and μ are the density, thermal expansion coefficient, thermal diffusivity and viscosity of the fluid, respectively, while ΔT is the temperature difference between characteristic vertical distance d, and g is the

acceleration of gravity. For sufficiently small *Ra*-numbers, the heat will be transferred through the fluid by *conduction* alone, in which macroscopic fluid motion is not produced. But when *Ra* exceeds a certain critical value Ra_c, macroscopic fluid motion called *convection* is set up. The first experimental investigations on thermal convection date back to Thomson (1881) and Bénard (1900), the latter of which has attracted greater attention due to the fascinating pattern of regular hexagonal cells. There are, however, varieties of convective patterns depending on the Rayleigh number, the Prandtl number $\mathrm{Pr} = \nu/\kappa$ ($\nu = \mu/\rho$ is the kinematic viscosity), the shape and aspect ratios of the container, the type of applied disturbances, the presence of surface tension, and so on.

2. Some Facet of Convective Patterns

2.1 Rayleigh-Bénard convection

The thermal convection in a horizontal fluid layer, in which the temperature of the lower boundary is kept higher than the upper boundary, has been studied extensively. The theory of thermal convection of this type was initiated by Rayleigh (1916), who assumed that the amplitude of the motion was infinitesimal such that the equations (Boussinesq equations) could be linearized. If the perturbations of velocity and temperature fields $\boldsymbol{v} = (u, v, w)$ and T are assumed in the form:

$$(u, v, w, T) = \big(U(z), V(z), W(z), T(z)\big)\exp\Big[i\big(k_x x + k_y y\big) + st\Big], \tag{1}$$

the problem is reduced to finding eigenfunctions satisfying the given boundary conditions, where x and y are the coordinate axes in the horizontal plane and z is the axis in the upward direction. Neutrally stable solution ($s = 0$) gives a relation between *Ra* and $k = \sqrt{k_x^2 + k_y^2}$, whose minimum value gives Ra_c. The theoretical value of the critical Rayleigh number Ra_c is 1707.7 for rigid-rigid boundaries, 1100.6 for rigid-free boundaries, and $27\pi^4/4$ (= 657.51) for free-free boundaries (Chandrasekhar, 1961, for review), which agree with experiments quite well. As far as the onset of convection and the wave number of the marginally stable mode are concerned, linearized theory is applied successfully. However, it is the absolute value k, and not each of its component k_x and k_y, that determine the value of Ra_c, so that any combination of k_x and k_y with the same wave number k is allowed. For instance, in terms of the solutions:

$$\big(w_1, w_2, w_3\big) = W(z)\Big\{\cos\big(k_x x + k_y y\big), \cos\big(k_x x - k_y y\big), \cos\Big(\sqrt{k_x^2 + k_y^2}\, y\Big)\Big\}, \tag{2}$$

the combinations $w_1 \pm w_2$ give bimodal convection with square cells, which

include two-dimensional rolls as a special case, while $w_1 + w_2 + w_3$ with $k_x = (\sqrt{3}/2)k$ and $k_y = k/2$ gives regular hexagonal cells. Superposition of these modes with suitable magnitudes leads to variety of convective patterns, as was confirmed experimentally by applying suitable initial disturbances. We shall show some examples of convective cells in Figs. 1–3. Figures 1a and 1b show almost two-dimensional and concentric rolls, respectively, in a circular container, which were obtained with controlled initial conditions (see also Busse and Whitehead, 1971, 1974). Contrary to this, we have rather irregular cells owing to isotropy in the horizontal directions under uncontrolled initial conditions. Figures 2a–2d are a sequence of photographs showing the formation of these cells at an *Ra*-number slightly larger than Ra_c. Small hexagonal cells of nearly the same size (Fig. 2b) merge with neighboring cells, which leads to a mixture of long snaky cells of arbitrary orientations and the remaining isolated smaller cells (Figs. 2d and 2e). Near a lateral boundary, the rolls tend to be parallel to the wall, which is the only source of finite disturbance to an otherwise homogeneous temperature field. Figures 3a–3c are also pictures taken under uncontrolled initial condition in a circular vessel at $Ra \approx Ra_c$. Initially, concentric-roll-like cells are formed, which develop into a long spiral cell through merging. Concentric cells in a circular vessel or rolls along any shape of the boundary wall, in uncontrolled case, have been shown by Koschmieder (1974), where the convective motion is initiated at the side walls at subcritical *Ra*-number and developed into the interior region.

Nonlinear theory or non-Boussinesq approximation is necessary to give the selection rule for convective patterns slightly above Ra_c in a fluid layer of (nearly) infinite extent. For example, if the basic temperature field has vertically nonlinear gradient, or if the kinematic viscosity ν depends nonlinearly on temperature T, subcritical stable hexagonal cells appear ($Ra = R_{-1}$), followed by two-dimensional rolls ($Ra = R_1$), as shown schematically in Fig. 4. In certain *Ra*-numbers ($R_1 < Ra$

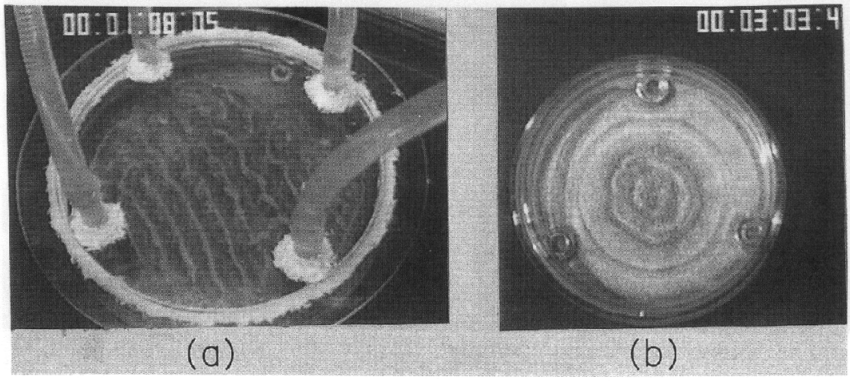

Fig. 1. (a) Two-dimensional and (b) axisymmetric rolls, obtained in a thin horizontal fluid layer in a circular container with controlled initial conditions.

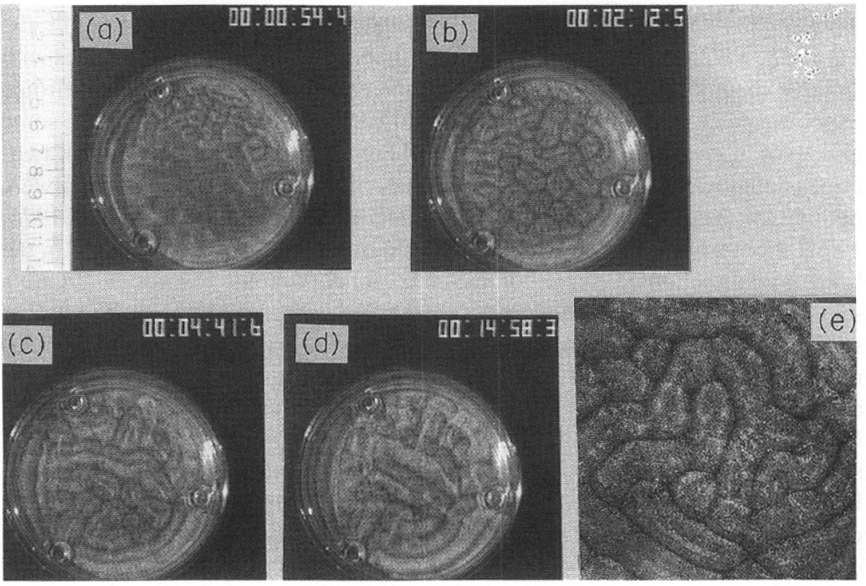

Fig. 2. Sequence of photographs at (a) $t \approx 1$ min, (b) $t \approx 2$ min, (c) $t \approx 5$ min and (d) $t \approx 15$ min, showing the formation of convection cells in a horizontal fluid layer at Ra-number slightly larger than Ra_c (uncontrolled). (e) Mixture of long winding rolls and small isolated cells, which are formed through merging with neighboring cells.

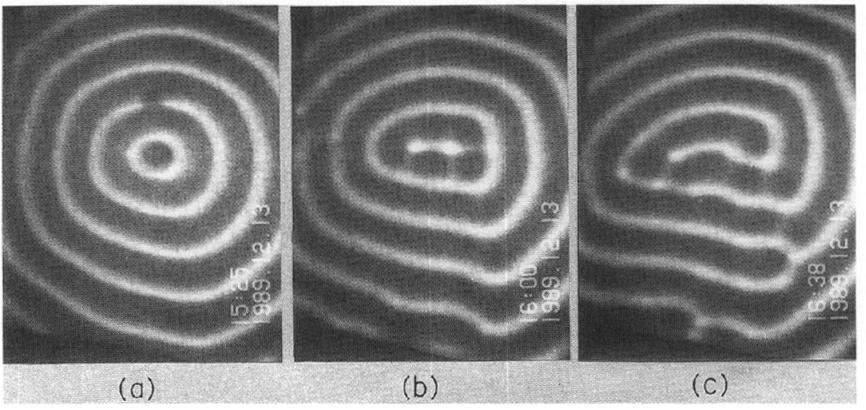

Fig. 3. An example of pattern change from concentric to spiral cells through merging, which was observed in a circular container at $Ra \approx Ra_c$ with uncontrolled initial condition.

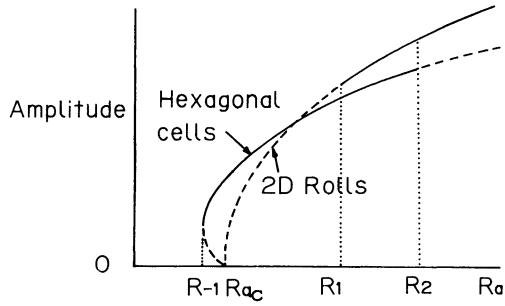

Fig. 4. Schematic diagram showing the selection of convective patterns in an infinitely large horizontal fluid layer in nonlinear theory. The solid and broken lines correspond to stable and unstable states, respectively.

$< R_2$), both types of cells coexist. For detail, see Segel and Stuart (1962) and Palm (1975).

2.2 Prandtl number dependence

Figure 5 shows schematically the dependence of the Prandtl number and the Rayleigh number on the observed cell patterns in a horizontal fluid layer with

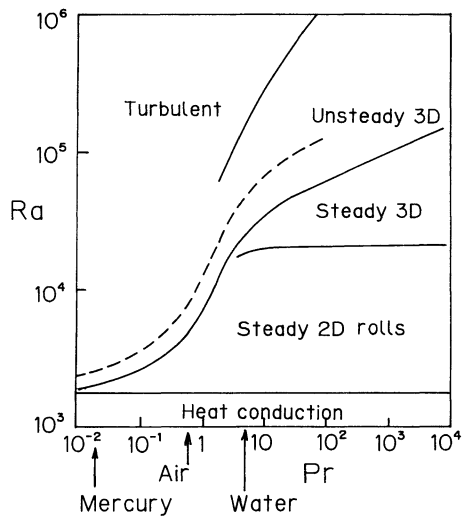

Fig. 5. Schematic diagram showing the dependence of Rayleigh number and Prandtl number on the convective patterns in an infinitely large horizontal fluid layer.

large aspect ratio Γ (=horizontal length of the container/depth of the fluid layer). In low Pr number fluid such as air ($Pr \sim 1$), a sequence of transitions: heat conduction state without macroscopic motion (HC) $\rightarrow$ steady two-dimensional rolls (S2D) $\rightarrow$ unsteady three-dimensional forms (U3D) $\rightarrow$ turbulent convection (TC), occurs with the increase of Ra. On the other hand, in a liquid like water ($Pr \sim 7$), steady three-dimensional convections (S3D) appear between S2D and U3D, which complicates the convective pattern significantly. For details, see Krishnamurti (1970, 1973), Busse and Whitehead (1971, 1974) and Busse (1981).

2.3 Thermal convection in finite aspect ratio

If the fluid layer is confined in a container of finite aspect ratio, the resulting convection will be greatly influenced by the geometry of the boundary wall. There have been many experiments to check the effect of aspect ratio, especially by measuring Ra_c and wavelength, from which the reasonable approximation to an infinite layer has been argued (see Koschmieder, 1974, for review). For convections in a vessel of very small aspect ratio, the degrees of freedom are neccessarily small owing to the presence of the side walls. Indeed the thermal convection observed in a rectangular box of small aspect ratios, in which the lower wall is kept at higher temperature than the upper wall, is the two-dimensional rolls with their axes parallel to the shorter side of the container (Davis, 1967; Stork and Müller, 1972). Extensive studies have been made for these two decades on the evolution of the time dependence of convection in this geometry, which have revealed several routes to chaotic states: (a) route to chaos via period doubling bifurcation (subharmonic bifurcation), which is theoretically studied by Feigenbaum (1979) and is experimentally confirmed by Libchaber and Maurer (1980), Gollub and Benson (1980), Giglio *et al.* (1981), among others, (b) route to chaos via intermittency (Pomeau and Manneville, 1980; Dubois *et al.*, 1983), (c) route to chaos via quasiperiodic oscillation, which is sometimes associated with phase-locking, or the appearance of the three incommensurate frequencies (Ruelle and Takens, 1971; Newhouse *et al.*, 1978), which was evidenced by Gollub and Benson (1980), and (d) the sudden transition to chaos at critical Rayleigh number (Lorenz, 1963), which has not been observed experimentally in thermal convection in a box-like fluid region, as will be discussed in the next section.

2.4 Surface-tension-driven thermal convection

In the presence of a free surface, different type of convective motion can be caused by the variation of surface tension with temperature (Block, 1956; Pearson, 1958). The magnitude of this thermo-capillary flow is characterized by the Marangoni number : $Ma = (\partial\gamma/\partial T)\Delta T d/\kappa\mu$, where γ is the surface tension coefficient. The convective pattern is characterized by a regular array of hexagonal cells, as is shown in Fig. 6. The vertical velocity at the centre of each cell is upward or downward, depending on whether $\partial\gamma/\partial T$ is negative (as in most liquids) or positive (as in most gases), as was shown by Tippelskirch (1956). It was this type

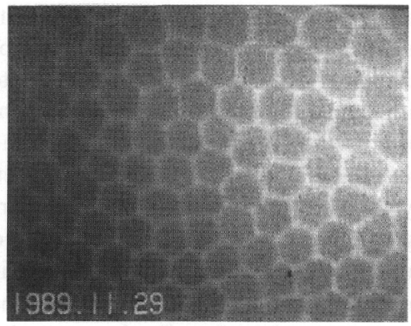

Fig. 6. Surface-tension-driven thermal convection, showing almost regular array of hexagonal cells.

of convective pattern that Bénard (1900) originally reported in his historical paper.

2.5 Bioconvective patterns

Rayleigh-Bénard convection occurs as a consequence of inversion of density distribution owing to negative temperature gradient. Essentially the same situation is achieved by the aggregates of micro-organisms, such as ciliated protozoan *Tetrahymena pyriformis*. This creature has a density slightly heavier than that of the surrounding fluid and a negative gyrotaxis. If they assemble in a thin layer near the surface, density inversion is created, and convective patterns of regularly spaced fingers, patches and hexagonal-cell-like sheets are formed (Winet and Jahn, 1972; Plesset and Whipple, 1974; Childress *et al.*, 1975). Similarly tall plumes or a series of "bulbous expansions" of micro-organisms spaced regularly in a suspension of a particular algal species (*Chlamydomonas nivalis*) were found by Kessler (1985) and are analysed by Pedley *et al.* (1988). Evolution of bioconvective pattern of different species (*Heterosigma akashiwo*) is also analysed by Harashima *et al.* (1988).

2.6 Geophysical and astrophysical convective patterns

The resemblance of cell patterns in Rayleigh's theory to certain forms of cloud, now obtained by infrared light photograph from satellites, was early noticed by meteorologists (Kimura, 1976; Tritton, 1977, for review). There are, however, many factors to be considered. One can fairly frequently observe clouds in long parallel evenly spaced lines. This might be two-dimensional convection rolls, as mentioned before, or shear instability owing to large gradient of winds in stably stratified air. These two processes can be distinguished by the orientation of roll axes with respect to the wind direction; convection cells are aligned along the wind, while billows across it. Concerning the convection cells, the horizontal

extent is as large as a few 100 km, while its vertical height is at most 10 km, so that the aspect ratio is much larger than that observed in laboratory experiments. This might be attributed to stratification, the release of latent heat, variation of material constants with temperature and pressure, and so on. Cellular convective patterns are also reported in the ocean (Stewart, 1969). The granular structure on the Sun's photosphere is considered to be very large convection cells with typical size 1000 km and typical life time 10 minutes. Doppler shift measurements revealed that the bright domains are ascending hotter regions, while the darker boundaries are descending colder regions. Thus the pattern is similar to that of the Rayleigh-Bénard convection, but the boundary conditions might be quite different reflecting the interior structure of the Sun. Furthermore, the flow within the cell is highly turbulent with extremely large Rayleigh number, which makes it difficult to compare quantitatively with laboratory experiment.

3. Cellular Structure in Thermal Convection in a Vertical Tours

We shall confine our attention to convections in a torus, in which the plane containing the tube centreline is placed vertically in a vertically uniform negative temperature gradient. The fluid motion in this region is intuitively considered to be the simplest, because it has only two characteristic lengths a (tube radius) and R (loop radius), and one-dimensional flow along the loop is expected. Contrary to this, the fluid motion in a spherical container, which is much simpler in geometry, will be axisymmetric or three-dimensional, so that it will be hydrodynamically more complicated. The thermal convection in a torus, however, is found to have possibilities of a variety of fluid motion at higher Rayleigh numbers in spite of the simplicity of the geometry (Keller, 1966; Welander, 1967; Mulkus, 1972), including the behaviour described by the Lorenz model (Lorenz, 1963; Yorke and Yorke, 1981), the latter being a useful pedagogical example of nonlinear dynamics. Besides academic interests, this system has important practical applications to heat transfer problems in engineering such as toroidal thermosyphon or solar water heater, cooling devices in nuclear reactors, and so on.

Several experiments have been made (Creveling *et al.*, 1975; Gorman *et al.*, 1984, 1986; Stern and Greif, 1987; Widmann *et al.*, 1989; Suda and Mimura, 1989; Ehrhard and Müller, 1990), and some of their results resemble the one-dimensional Lorenz-like behaviour, in which the fluid motion is necessarily "turbulent". There seems to be a wide gap between their experimental set up and the assumptions made in deriving the Lorenz model. In contrast to these experiments, we have observed cellular structures (Sano, 1984, 1986, 1989, 1991a; Sano and Wakayama, 1989) in thinner tori, in which better approximation to vertically uniform temperature gradient is met. Our experiments show the transition from laminar quasi-one-dimensional flow to three-dimensional flow with cellular structure, in which nonuniformities of temperature and velocity

owing to the finiteness of thermal conductivity of the fluid play important roles.

3.1 Experimental apparatus

Two kinds of thin toroidal loops with cross sectional diameter $2a = 1$ cm and 0.5 cm (hereafter referred to as torus I and torus II), each having a total loop length of $2\pi R = 100$ cm and a wall thickness of 1 mm, were used. The aspect ratio $\varepsilon = a/R$, which is an indicator of realizability of one-dimensional flow, is both very small (= 0.0314 and 0.0157, for torus I and torus II, respectively). The loop, which is made of Pyrex glass, is placed vertically. The upper and lower parts of the torus are partially covered by jackets made of plexiglass (each jacket surrounds one quarter of the total loop length), into which cooling and heating water, respectively, are supplied at a constant rate (Fig. 7). The remaining parts of the loop are exposed to air at room temperature. This apparatus, in which the temperature on the tube wall is well defined, is designed to achieve better approximation to a vertically uniform temperature gradient than previous experiments. The entire apparatus can be rotated around the centre of the torus in a vertical plane, so that the right-and-left symmetry of the loop could be carefully checked. The temperatures of the cooling and heating water were kept constant within an accuracy of ±0.1°C, while the room temperature was regulated within an accuracy of ±0.5°C. The working fluids used in the present work were distilled water and ethyl alcohol (99.5%). Combined use of different tori and different liquids enables us to cover a wide range of Rayleigh number region. We visualized the whole flow field and

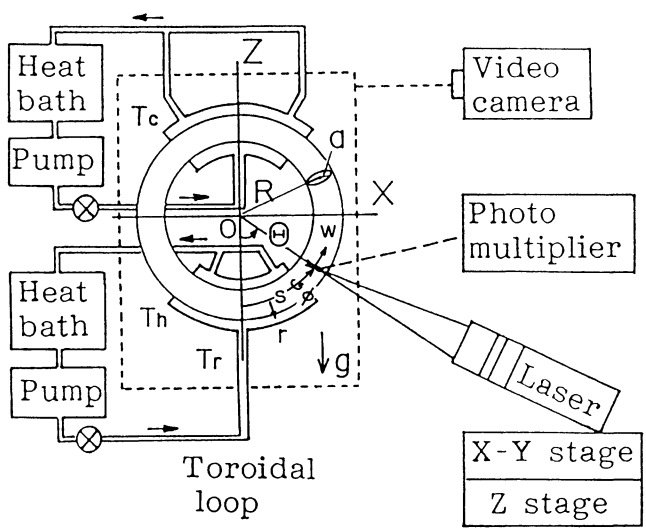

Fig. 7. A sketch of our experimental apparatus and the definition of the coordinate system.

temperature distribution, and measured the velocity field directly by means of a laser Doppler velocimeter (LDV).

3.2 Experimental results

3.2.1 Critical Rayleigh number for the onset of convection

We show the Reynolds number squared against the Rayleigh number in Fig. 8. Here the Reynolds number is defined by $Re = 2aU/\nu$, where U is the maximum longitudinal velocity in the cross section of the tube. This figure shows that they can be accurately fitted by different but single straight lines with the same intercept Ra_c, so that Re is proportional to $\sqrt{Ra - Ra_c}$. The experimentally determined critical Rayleigh number Ra_c is about 35, and this relation holds for an Ra-number range up to a few hundreds. This power law near the critical Rayleigh number has been derived in many critical phenomena described by mean-field theory as well as in nonlinear stability theory in fluid dynamics, and in particular in the Lorenz model. Surprisingly, this power law is followed far beyond the threshold of the convective motion as shown in Fig. 8.

3.2.2 Steady cellular flow

As the Rayleigh number was further increased (greater than about 800 in water in torus I), a local recirculating flows manifested itself in each quadrant of the loop like those shown in Fig. 9. The generation of this pattern is as follows: A heated lighter fluid element, initially moving upwards along the upper wall in

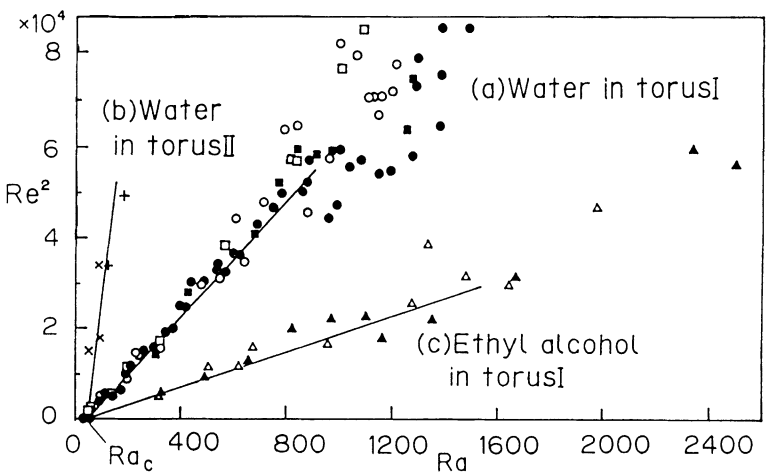

Fig. 8. Relation between Ra and Re^2: (a) anti-clockwise flow of water in torus I(○, □); clockwise flow of water in torus I(●, ■), (b) anti-clockwise flow of water in torus II(×); clockwise flow of water in torus II (+), (c) anti-clockwise flow of ethyl alcohol in torus I(△); clockwise flow of ethyl alcohol in torus I (▲).

the lower half of the loop (①), departs to the upper side of the wall in the upper half of the torus (②), while a colder fluid element moves downward along the opposite side of the tube wall in opposite direction (③ and ④), so that these two currents cross at positions $\Theta \approx \pm 90°$ (⑤, see the photograph of Fig. 9b, where the blue streakline moves downward, while red one goes upward). Here Θ is measured counter-clockwisely along the loop from the bottom. At $\Theta \approx 0°$ or 180° the flows with the same direction connect smoothly (⑥), and circulatory flows which twists at these four positions are formed. The presence of cellular region is quantitatively confirmed by measuring the velocity field in terms of an LDV, as well as by analysing the visualization picture of the fluid motion by means of tracer particles. This cellular motion is sometimes obscured by the presence of Poiseuille-like main flow, so that the number and positions of the cells are sensitively influenced by the symmetry of the system, as was shown in our previous papers (Sano, 1984, 1986, 1989, 1991a; Sano and Wakayama, 1989).

3.2.3 Time dependence of the cellular structure

The velocity component w_M along the loop (torus I) in ethyl alcohol at $r/a = 0.2$ and $\Theta = -77°$ was measured by an LDV, where r is the distance in the cross section of the tube from the centreline (see Fig. 12). The flow became oscillatory at $Ra \gtrsim 2500$ in this test liquid, and sizes and positions of cellular substructure were observed to fluctuate. We have also checked the spectrum, the two-dimensional phase portrait, and the Poincaré section of the corresponding data (Sano, 1991a). The flow was almost stationary at $Ra = 2330$ ($\approx 67\, Ra_c$). The first Hopf bifurcation, i.e., transition from a stationary to a periodic flow with frequency f_1 (and perhaps its higher harmonics) was easily recognized at a certain Ra value between 2330 and 2620 ($\approx 75\, Ra_c$). As the Rayleigh number was further increased, the second Hopf bifurcation with frequency f_2 appeared. All sharp peaks in the spectrum could be identified as linear combinations of two basic frequencies of the form $mf_1 + nf_2$, where m and n are integers, $f_1 = 155$ mHz and $f_2 = 90$ mHz at $Ra = 2910$ ($\approx 83\, Ra_c$). The ratio $f_2/f_1 = 1.72$ is close to $\sqrt{3}$, suggesting that the two frequencies are incommensurate. Indeed the orbit in the phase space was close to a torus in spite of considerable scattering of the data. As far as the spectrum is concerned, frequency locking seemed to occur at $Ra \approx 3000$ ($\approx 86\, Ra_c$). This phase-locking state seemed to be unstable, and the locking ratio could not be reproduced exactly, probably because of the coarseness of our Ra-number scans and the presence of the noise. At $Ra = 3210$ ($\approx 92\, Ra_c$), the velocity signal looked erratic, and broadband spectra developed, which indicate nonperiodic motion of the fluid. For $Ra \gtrsim 3500$, streaklines began to be irregularly twisted, and the velocity field was highly turbulent at positions where the counter flows met. Experiments were carried out up to $Ra = 10460$, using ethyl alcohol. The magnitude of the velocity increased in both directions, but large scale structures still remained. In our experiment, "reversal of flow directions" was not observed in its literal sense, rather the magnitude of cellular flow or bi-directional flows was

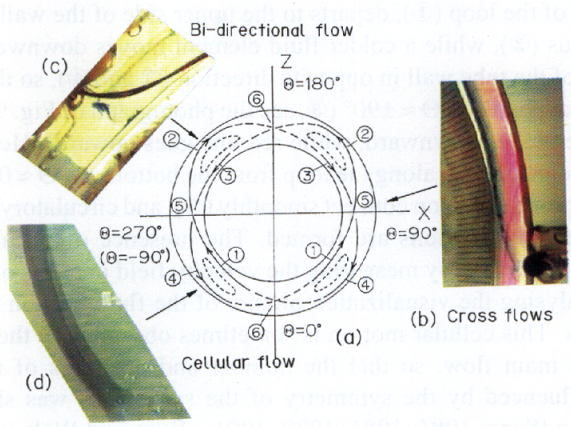
Bi-directional flow
(c)
Z
Θ=180°
X
Θ=90°
Θ=270°
(Θ=-90°)
Θ=0°
(a)
(b) Cross flows
(d)
Cellular flow

Fig. 9

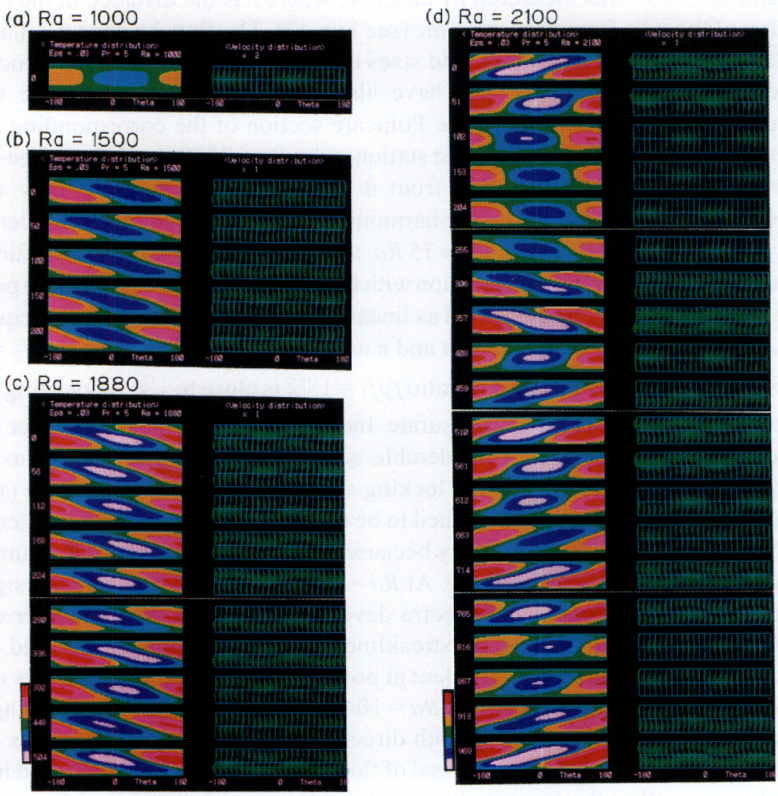
(a) Ra = 1000
(b) Ra = 1500
(c) Ra = 1880
(d) Ra = 2100

Fig. 14

found to change in time.

All these findings show that the transition from a steady unidirectional flow to more complex ones occurs through a process which is quite different from that expected in the Lorenz model. It seems to be rather closely described by a route to chaos via quasiperiodic state, in which three-dimensional structure changes both spatially and temporally.

3.3 Theoretical analysis

We have shown experimentally that the simple one-dimensional model of the Lorenz type should be modified so as to include three-dimensionality of the flow fields for the purpose of accurately predicting the fluid motion. Some extensions of the Lorenz model to take into account of the three-dimensionality have been made by Yorke *et al.* (1987), which have made allowance for radial variations of temperature, and introduced axially symmetric higher order spatial modes in their expansion. Their assumptions, however, seems unrealistic. In this section, we shall take into account several types of convective flows with spatial structure which can explain the experimentally observed flow patterns (Sano, 1986, 1987, 1988, 1989, 1991b).

3.3.1 Mathematical formulation of the problem

We take the x and z axes in the plane of the generator of the torus with z axis in the negative direction of gravity (see Fig. 7). We also introduce the coordinate system (r, ϕ, s), where s is the distance measured counter-clockwisely from the bottom along the generator, while (r, ϕ) is the polar coordinate system in the cross section. The direction of $\phi = 0$ is chosen so that it always coincides with the direction from the generator to outer edge of the torus in the plane of the ring (x-z plane). We analyse the fluid motion on the basis of the Boussinesq approximation so that the governing equations for the velocity $\boldsymbol{v}$, temperature T and pressure p are

$$\nabla \cdot \boldsymbol{v} = 0, \tag{3a}$$

Fig. 9. (a) Generation of cellular pattern (schematic). Visualization picture of (b) streaklines (blue for downward, and red for upward motions) showing cross flows, (c) a timeline showing bi-directional flow, and (d) steady separated region.

Fig. 14. Temperature and velocity distributions in the plane of the ring at (a) $Ra = 1000$, (b) $Ra = 1500$, (c) $Ra = 1880$, and (d) $Ra = 2100$, with $Pr = 5$ and $\varepsilon = 0.03$, exhibited by ELM8. The number and positions of the cells as well as the temperature distributions shift (b) periodically and (c) quasiperiodically, while (d) higher temperature fluid region extends its tongue-like domain either to the upper left region or to the upper right region non-periodically inside the loop.

$$\rho_0\left(\frac{\partial}{\partial t}\boldsymbol{v}+\boldsymbol{v}\cdot\nabla\boldsymbol{v}\right)=-\nabla p+\mu\Delta\boldsymbol{v}-\rho_0\left[1-\alpha\left(T-T_0\right)\right]g\boldsymbol{e}_z, \tag{3b}$$

$$\frac{\partial}{\partial t}T+\boldsymbol{v}\cdot\nabla T=\kappa\Delta T, \tag{3c}$$

where ρ_0 is the density of the fluid at temperature T_0, and $\boldsymbol{e}_z$ is an upward unit vector. We take the steady heat conduction state under a constant vertical temperature gradient $-\beta$ as a fundamental solution. The perturbed fields satisfy the linear equations, which are expressed in terms of the (r, ϕ, s) coordinate system. Hereafter, we shall only deal with a thin loop ($\varepsilon << 1$).

In order to analyse general situations including both symmetric and antisymmetric modes, which are caused by experimentally uncontrollable small disturbances under symmetric boundary conditions, we expand all quantities in terms of the double Fourier series in ϕ and Θ in either of the following four types:

(i) S-type;

$$\begin{aligned}&\left(T,p/Pr,u\right)=\sum\left(T_{mn}^{S}(r),P_{mn}^{S}(r),U_{mn}^{S}(r)\right)\cos m\phi\cos n\Theta,\\&w=\sum W_{mn}^{S}(r)\cos m\phi\sin n\Theta,\quad v=\sum V_{mn}^{S}(r)\sin m\phi\cos n\Theta,\end{aligned} \tag{4a}$$

(ii) A-type;

$$\begin{aligned}&\left(T,p/Pr,u\right)=\sum\left(T_{mn}^{A}(r),P_{mn}^{A}(r),U_{mn}^{A}(r)\right)\cos m\phi\sin n\Theta,\\&w=\sum W_{mn}^{A}(r)\cos m\phi\cos n\Theta,\quad v=\sum V_{mn}^{A}(r)\sin m\phi\sin n\Theta,\end{aligned} \tag{4b}$$

(iii) $\tilde{\mathrm{S}}$-type;

$$\begin{aligned}&\left(T,p/Pr,u\right)=\sum\left(T_{mn}^{S}(r),P_{mn}^{S}(r),U_{mn}^{S}(r)\right)\sin m\phi\cos n\Theta,\\&w=\sum W_{mn}^{S}(r)\sin m\phi\sin n\Theta,\quad v=\sum V_{mn}^{S}(r)\cos m\phi\cos n\Theta,\end{aligned} \tag{4c}$$

(iv) $\tilde{\mathrm{A}}$-type;

$$(T, p/Pr, u) = \sum \left(T^A_{mn}(r), P^A_{mn}(r), U^A_{mn}(r)\right) \sin m\phi \sin n\Theta,$$

$$w = \sum W^A_{mn}(r) \sin m\phi \cos n\Theta, \quad v = \sum V^A_{mn}(r) \cos m\phi \sin n\Theta, \tag{4d}$$

where $\sum$ denotes summation over m, $n = 0, 1, 2, \ldots$, and (u, v, w) are the velocity components in the (r, ϕ, s) directions, respectively. By substituting either one of the expressions (4a)–(4d) for our linear equations, we obtain an infinite set of ordinary differential equations for T_{mn}, W_{mn}, U_{mn}, V_{mn} and P_{mn}, in each corresponding type. Convergence of these series solution is assumed.

3.3.2 Onset of convection

We first consider the simplest A-type flow which is given by the series: $W^A{}_{00}$-$T^A{}_{01}$-$W^A{}_{02}$-$T^A{}_{03}$-... By substituting this series for linear equations, and by assuming the solution of the form:

$$W^A_{0m} = a_m J_0\left(k_{0q} r\right), \quad T^A_{0n} = b_n J_0\left(k_{0q} r\right), \quad (m = 0, 2, 4, \ldots, \; n = 1, 3, 5, \ldots), \tag{5}$$

(where J_i is the Bessel function of the first kind of order i, and k_{iq} is the q-th zero point of J_i), we obtain after some calculation

$$a_{2N} = \left(p^N + \frac{1}{p^N}\right) a_0, \quad b_{2N+1} = \frac{\left(p^{2N+1} - 1\right) 2k^2_{0q} a_0}{p^N (p-1) Ra} \tag{6}$$

where $p + (1/p) = 2 - \alpha_0$. If we truncate the series at a certain large number of terms by putting $a_{2N} = 0$, we have the conditions for α_0, which give the eigenvalues Ra^* of the Rayleigh numbers. The minimum value of $Ra^*_{\min}$ $(= Ra_0)$ for $N \to \infty$ is

$$Ra_0 = k^4_{01} = 33.44523\ldots, \tag{7}$$

where $k_{01} = 2.404825\ldots$ is the first zero of J_0. This figure agrees fairly well with the experimentally determined critical Rayleigh number Ra_c. The first pair of terms ($W^A{}_{00}$, $T^A{}_{01}$) corresponds to a Poiseuille-like flow along the loop, which we shall term A_{00}-mode (Fig. 10a);

$$\left(A_{00}\right): \; T = A J_0\left(k_{01} r\right) \sin\Theta, \quad w = A k^2_{01} J_0\left(k_{01} r\right), \quad u = v = 0, \tag{8}$$

where A is an arbitrary constant.

3.3.3 Some other typical steady convective patterns

We shall show some typical convective flows, which are obtained similarly

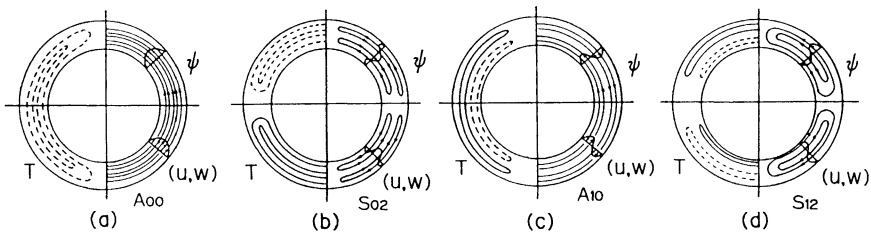

Fig. 10. Velocity and temperature fields of some basic modes. The right half of each picture shows schematic streamlines ψ and velocity components (u, w) in the plane of the ring, while the left half shows isotherms (solid and broken lines correspond to positive and negative values, respectively).

to the previous subsection:

$$
\begin{aligned}
&(S_{02}):\quad T=\left[J_0(kr)+(J_0/I_0)I_0(kr)-2J_0\right]\cos\Theta,\\
&w=2k^2\left[J_0(kr)-(J_0/I_0)I_0(kr)\right]\sin 2\Theta,\\
&u=-4\varepsilon k\left[J_1(kr)-(J_0/I_0)I_1(kr)\right]\cos 2\Theta,\\
&p/Pr=2\varepsilon^{-1}k^4J_0\cos 2\Theta,
\end{aligned}
\tag{9}
$$

where $J_n = J_n(k)$, $I_n = I_n(k)$, and $k = 4.6108998...$ is the first zero of $I_0(k)J_1(k) - J_0(k)I_1(k) = 0$, as shown in Fig. 10b;

$$
\begin{aligned}
&(A_{10}):\quad T=AJ_1(k_{11}r)\cos\phi\sin\Theta,\\
&w=Ak_{11}^2J_1(k_{11}r)\cos\phi,\quad u=v=0,
\end{aligned}
\tag{10}
$$

where $k_{11} = 3.831706...$ is the first zero of J_1. Note that Eqs. (10) describe the anti-parallel Poiseuille-type flow along the loop (Fig. 10c);

$$
\begin{aligned}
&(S_{12}):\quad T=T_B(r)\cos\phi\cos\Theta,\quad w=W_B(r)\cos\phi\sin 2\Theta,\\
&u=U_B(r)\cos\phi\cos 2\Theta,\quad v=V_B(r)\sin\phi\cos 2\Theta,
\end{aligned}
\tag{11}
$$

$$p / Pr = P_B(r)\cos\phi\cos 2\Theta,$$

where

$$T_B = -AJ_1(k_{11}r),\quad W_B = -2k_{11}^2 AJ_1(k_{11}r),$$

$$U_B = \varepsilon A\left\{2k_{11}J_0(k_{11})(1-r^2) + 4J_1(k_{11}r)/r - 4k_{11}\left[J_0(k_{11}r) - J_0(k_{11})\right]\right\}, \tag{12}$$

$$V_B = \varepsilon A\left[-6k_{11}J_0(k_{11})(1-r^2) + 4J_1(k_{11}r)/r\right],$$

$$P_B = \varepsilon A\left[-16k_{11}J_0(k_{11})r + 4k_{11}^2 J_1(k_{11}r)\right],$$

as shown in Fig. 10d. This mode describes a symmetric four-cell-type three-dimensional convection. There are many other modes of interest, which are shown in our previous papers (Sano, 1987, 1988, 1991b)

3.3.4 Superposition of basic patterns

We have seen that A_{00}-mode describes the steady flow along the loop at Rayleigh number region slightly above Ra_c, and that S_{12}-mode represents flow with four cells. In this subsection, we shall briefly consider superpositions of symmetric and antisymmetric flows in order to describe the experimentally observed flow patterns.

(a) $(S_{12}) + \varepsilon^*(A_{00})$:

Superposition of small amount of S_{12} on A_{00} leads to a circulatory flow along the loop, in which the position of the highest velocity in the cross section deviates from a circle (Fig. 11a). With the increase of S_{12} mode, four cells become discernible. If anti-clockwise (A_{00})-type flow is accompanied, the cells in the first and third quadrant shift toward the inner wall, while those in the second and fourth

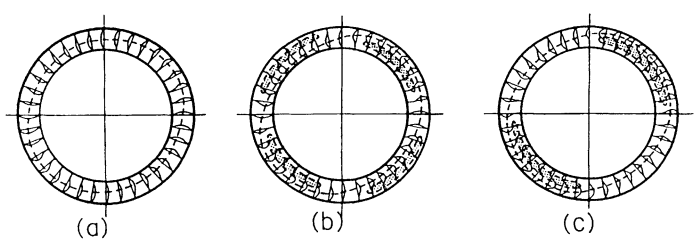

Fig. 11. Superposition of basic modes; (a) S_{12}:A_{00} = 0.2:1, (b) S_{12}:A_{00} = 0.5:1, (c) S_{12}:A_{00}:A_{10}= 0.5:1:0.5. Dotted lines illustrate particle paths.

quadrant shift toward the outer wall of the torus (Fig. 11b). This result is in agreement with our observation.

(b) $(S_{12}) + \varepsilon^*(A_{00}) + \varepsilon^{**}(A_{10})$

Superposition of these three types gives steady flow with two cells (Fig. 11c), which is often observed experimentally at higher Rayleigh number regions when a slight asymmetry was introduced.

3.3.5 Time dependence of the superposed patterns

We shall now derive model equations to describe time dependence of the flow and temperature fields. We employ four modes mentioned above to represent experimentally observed flow field, whose amplitudes are assumed to be functions of time. Thus we have

$$w = X(t)W_{00}^A + A(t)W_{02}^S \sin 2\Theta + B(t)W_{10}^A \cos\phi + C(t)W_{12}^S \cos\phi \sin 2\Theta, \tag{13}$$

$$T = Y(t)T_{01}^A \sin\Theta + Z(t)T_{01}^S \cos\Theta + D(t)T_{11}^A \cos\phi \sin\Theta + E(t)T_{11}^S \cos\phi \cos\Theta,$$

and similarly for u, v and p. By substituting these expressions for Eqs. (3a)–(3c), and equating like terms, we have, after some calculation (Sano, 1991b), a set of first order nonlinear differential equations for X, A, B, ..., and E:

$$\dot{X} = -5.7832PrX + 0.086458PrY, \tag{14a}$$

$$\dot{A} = -(15.265 + 20.291Pr)A + 0.019666PrZ, \tag{14b}$$

$$\dot{B} = -14.682PrB + 0.034055PrD, \tag{14c}$$

$$\dot{C} = -14.682PrC + 0.017028PrE, \tag{14d}$$

$$\dot{Y} = 5.7832(RaX - Y) + \varepsilon(7.9025XZ - 15.055AY + 0.98507BE + 12.641CD) \tag{14e}$$

$$\dot{Z} = 12.714(RaA - Z) + \varepsilon(-5.7051C - 3.7635XY + 11.841AZ - 0.67980BD - 8.7237CE) \tag{14f}$$

$$\dot{D} = 14.682(RaB - D) + \varepsilon(5.4535XE - 33.883AD + 20.062BZ - 25.831CY) \tag{14g}$$

$$\dot{E} = 14.682(RaC - E) + \varepsilon(10.929A - 5.4535XD + 33.883AE - 13.845BY + 61.536CZ). \quad (14h)$$

As is easily shown, the above equations are reduced to the Lorenz model when only the terms X, Y and Z are retained:

$$\dot{X} = -PrX + PrY, \quad \dot{Y} = (Ra / Ra_c)X - Y + XZ, \quad \dot{Z} = -bZ - XY, \quad (15a,b,c)$$

where b is a geometrical parameter and the sign of Z has been reversed. In this context, the model equations (14a)–(14h) can be regarded as an extended Lorenz model with eight variables (ELM8).

Numerical simulation was made for changing Ra with fixed $\varepsilon = 0.03$ and $Pr = 5$. The global characters of the orbits in phase space with the same ε, Pr and Ra but with different initial conditions are similar to each other. Figure 12 are typical velocity signals $\hat{w}_M$ obtained by ELM8, where $\hat{w}_M$ is the velocity w at $r/a = 0.2$,

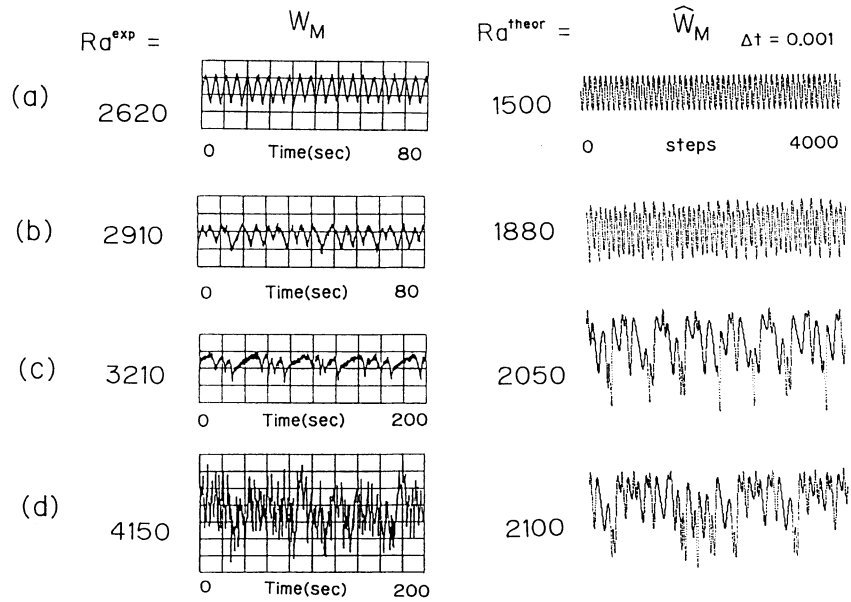

Fig. 12. Rayleigh number dependence on the velocity component along the loop w_M (experimental, with $\varepsilon = 0.0314$, $Pr = 15$) and $\hat{w}_M$ (theoretical, with $\varepsilon = 0.03$, $Pr = 5$); (a) monoperiodic ($Ra^{exp} = 2620$, $Ra^{theor} = 1500$), (b) quasiperiodic ($Ra^{exp} = 2910$, $Ra^{theor} = 1880$), (c) chaotic($Ra^{exp} = 3210$, $Ra^{theor} = 2050$), and (d) highly chaotic($Ra^{exp} = 4150$, $Ra^{theor} = 2100$).

$\phi = 0°$ and $\Theta = 45°$. Experimental data w_M are also shown for comparison. The results of the numerical calculation can be summarized as follows:

(a) Thermal convection starts at $\hat{Ra}_c = 66.890$. Note that we have employed a truncated solution Eq. (8), which results in the critical Rayleigh number twice as large as Ra_0 shown in Eq. (7).

(b) The relation $\hat{w}_M \propto \sqrt{Ra - \hat{Ra}_c}$ is well fitted up to $Ra \sim 300$. The exponent changes gradually from 1/2 to 1, so that $\hat{w}_M \propto Ra$ for $Ra \gtrsim 1000$. Velocity field is steady, but three-dimensionality increases with Ra.

(c) First Hopf bifurcation occurs at $Ra = 1240$ (= 37.1 Ra_0), and periodic flow with frequency f_1 appears (Fig. 12a).

(d) Second Hopf bifurcation occurs at $Ra = 1810$ (= 54.1 Ra_0), with frequency f_2 (Fig. 12b). All sharp peaks can be interpreted by the combination of two frequencies f_1 and f_2 of the form $mf_1 + nf_2$, where m and n are integers.

(e) At some particular Ra values, frequency locking is observed. For example, we have found $f_L/f_2/f_1 = 1/7/15$ at $Ra = 1901$, $f_L/f_2/f_1 = 1/6/13$ at $Ra = 1929$, and $f_L/f_2/f_1 = 1/5/11$ at $Ra = 1995$, etc., where f_L is the locking frequency.

(f) At $Ra = 1996$ (= 59.7 Ra_0) the spectrum becomes broad. The Lyapunov exponent becomes positive, and the orbit looks chaotic (Figs. 12c and 12d).

(g) The present model shows numerical divergence at $Ra = 2308$ (= 69.0 Ra_0).

Behaviours for $Pr = 7$, 10 and 15 are similarly checked, which shows similar sequence of transitions, namely the route to chaos through quasiperiodic states (see the bar graphs in Fig. 13).

Figures 14a–14d show the temperature and velocity fields at some particular Ra-values. The torus is cut at $\Theta = 180°$ (top of the loop), and extended for compactness. Higher temperature corresponds to red region, while lower one

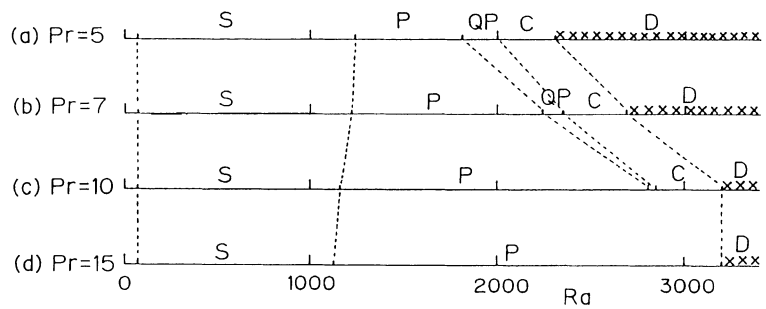

Fig. 13. Bar graphs of various instabilities in ELM8 with $\varepsilon = 0.03$ and (a) $Pr = 5$, (b) $Pr = 7$, (c) $Pr = 10$ and (d) $Pr = 15$. Symbols used are (S) steady; (P) periodic; (QP) quasiperiodic; (C) chaotic; and (D) numerical divergence.

corresponds to white and blue in the left half of each figure. Patterns change from above to below (except Fig. 14a which is in steady state). Note that cellular regions appear or disappear, or shift their positions periodically in Fig. 14b, quasiperiodically in Fig. 14c and non-periodically in Fig. 14d.

3.4 Comparison of our theory with experiment

Our theory on the onset of thermal convection, in terms of an infinite Fourier series, quantitatively agrees with experimental result of Ra_c (Subsection 3.3.2). Steady cellular flows are also described by superposition of several fundamental modes analysed in Subsections 3.3.2–3.3.4. Our model ELM8 shows qualitative agreement with experimentally observed sequence of dynamical regimes, i.e. steady, monoperiodic, quasiperiodic and chaotic states. ELM8 predicts frequent appearance of phase-locking states among quasiperiodic region, for which only a few evidence had been obtained in our experiment.

Disagreement of theoretical Ra value with experiment concerning the onset of oscillatory regime in $Pr = 15$ and $\varepsilon = 0.03$ for instance, which is about one half of experimentally found Ra, is probably due to the crudeness of the present model. Similar detailed comparison shows that our theoretical prediction agrees with experiment quantitatively within a factor of 2 (Sano, 1991b). Precise determination of the range of various instabilities, thereby removing the computational divergence, would require a much more appropriate choice of the coefficients of $X, Y, ..., E$ in Eqs. (14a)–(14h). Furthermore, increasingly large number of modes would be required to describe an increasingly large degrees of freedom in fluid motion at large Rayleigh number regions, which is beyond the scope of the present approach.

4. Conclusion

We have seen many convective patterns, which are generated in different initial or boundary conditions. Patterns exhibited at Rayleigh numbers near Ra_c under controlled initial conditions, or those generated by surface tension, are regular and has been theoretically tractable. However, convective patterns obtained under uncontrolled initial conditions could be much complicated. At higher Rayleigh numbers, convective patterns are spatially and temporally much more involved, even in the simplest geometry of the vertically placed toroidal loop, as has been shown here. Our theory, in which only a small number of steady basic modes are used to describe the convection at higher Ra-number region and is semi-quantitatively confirmed by the experiment, will serve as a first step to study transitions and formation of patterns in thermal convection in more general situations.

Acknowledgement

The author expresses his cordial thanks to Professor R. Takaki for his encouragement throughout this work and to Mr. T. Wakayama for his experimental assistance.

REFERENCES

Bénard, H. (1900), Les tourbillons cellulaires dans une nappeliquide, Revue Gén. Sci. Pur. Appl., **11**, 1261–1271 and 1309–1328.

Block, M. J. (1956), Surface tension as the cause of Bénard cells and surface deformation in a liquid film, Nature, **178**, 650–651.

Busse, F. H. (1981), Transition to turbulence in Rayleigh-Bénard convection, *Hydrodynamic Instabilities and the Transition to Turbulence*, edited by Swinney, H. L. and Gollub, J. P., pp. 97–137, Springer-Verlag.

Busse, F. H. and Whitehead, J. A. (1971), Instabilities of convection rolls in a high Prandtl number fluid, J. Fluid Mech., **47**, 305–320.

Busse, F. H. and Whitehead, J. A. (1974), Oscillatory and collective instabilities in large Prandtl number convection, J. Fluid Mech., **66**, 67–79.

Chandrasekhar, S. (1965), *Hydrodynamic and hydromagnetic stability*, Oxford, Clarendon Press.

Childress, S., Levandowsky, M., and Spiegel. E. A. (1975), Pattern formation in a suspension of swimming micro-organisms: equations and stability theory, J. Fluid Mech., **63**, 591–613.

Creveling, H. F., de Paz, J. F., Baladi, J. Y., and Schoenhals, R. J. (1975), Stability characteristics of a single-phase free convection loop, J. Fluid Mech., **67**, 65–84.

Davis, S. H. (1967), Convection in a box: linear theory, J. Fluid Mech., **30**, 465–478.

Dubois, M., Rubio, M. A., and Berge, P. (1983), Experimental evidence of intermittencies associated with a subharmonic bifurcation, Phys. Rev. Lett., **51**, 1446–1448.

Ehrhard, P. and Müller, U. (1990), Dynamical behaviour of natural convection in a single-phase loop, J. Fluid Mech., **217**, 487–518.

Feigenbaum, M. J. (1979), The universal metric properties of nonlinear transformations, J. Stat. Phys., **21**, 669–706.

Giglio, M., Musazzi, S., and Perini, U. (1981), Transition to chaotic behaviour via a reproducible sequence of period-doubling bifurcations, Phys. Rev. Lett., **47**, 243–246.

Gollub, J. P. and Benson, S. V. (1980), Many routes to turbulent convection, J. Fluid Mech., **100**, 449–470.

Gorman, M., Widmann, P. J., and Robbins, K. A. (1984), Chaotic flow regimes in a convection loop, Phys. Rev. Lett., **52**, 2241–2244.

Gorman, M., Widmann, P. J., and Robbins, K. A. (1986), Nonlinear dynamics of a convection loop: A quantitative comparison of experiment with theory, Physica, **19D**, 225–267.

Harashima, A., Watanabe, M., and Fujishiro, I. (1988), Evolution of bioconvective patterns in a culture of motile flagellates, Phys. Fluids, **31**, 764–775.

Keller, J. B. (1966), Periodic oscillations in a model of thermal convection, J. Fluid Mech., **26**, 599–606.

Kessler, J. O. (1985), Hydrodynamic focusing of motile algal cells, Nature, **313**, 218–220.

Kimura, R. (1976), On geofluiddynamics, Tenki, **23**, 591–612 (in Japanese).

Koschmieder, E. L. (1974), Bénard convection, Adv. Chem. Phys., **26**, 177–212.

Krishnamurti, R. (1970), On the transition to turbulent convection. Part 2. The transition to time-dependent flow, J. Fluid Mech., **42**, 309–320.

Krishnamurti, R. (1973), Some further studies on the transition to turbulent convection, J. Fluid Mech., **60**, 285–303.

Libchaber, A. and Maurer, J. (1980), Une experience de Rayleigh-Bénard de geometrie reduite: multiplication, accrochange et multiplication de frequences, J. Physique Collq., **C3-41**, 51–56.

Lorenz, E. N. (1963), Deterministic nonperiodic flow, J. Atmos. Sci., **20**, 130–141.

Mulkus, W. V. R. (1972), Non-periodic convection at high and low Prandtl number, Mem. Soc. Roy. Sci. Liege 6, **4**, 125–128.

Newhouse, S., Ruelle, D., and Takens, F. (1978), Occurrence of strange axiom A attractors near quasi-periodic flows on T^m, $m > 3$, Commun. Math. Phys., **64**, 35–40.

Palm, E. (1975), Nonlinear thermal convection, Ann. Rev. Fluid Mech., **7**, 39–61.

Pearson, J. R. (1958), On convection cells induced by surface tension, J. Fluid Mech., **4**, 489–500.

Pedley, T. J., Hill, N. A., and Kessler, J. O. (1988), The growth of bioconvection patterns in a uniform suspension of gyrotactic micro-organisms, J. Fluid Mech., **195**, 223–237.

Plesset, M. S. and Whipple, C. G. (1974), Viscous effects in Rayleigh-Taylor instability, Phys. Fluids, **17**, 1–7.

Pomeau, Y. and Manneville, P. (1980), Intermittent transition to turbulence in dissipative dynamical systems, Commun. Math. Phys., **77**,189–197.

Rayleigh, Lord (1916), On convection currents in a horizontal layer of fluids, when the higher temperature is on the under side, Phil. Mag., (6)**32**, 529–546 (Scientific papers (1920), Vol. 6, pp. 432–446, Cambridge Univ. Press, reprinted by Saltsman (1962)).

Ruelle, D. and Takens. F. (1971), On the nature of turbulence, Commun. Math. Phys., **20**, 167–192.

Sano, O. (1984), Experimental study on thermal convection in a torus. III, Nagare, **3**(Suppl.), 197–202 (in Japanese).

Sano, O. (1986), Thermal convection in a vertical torus, Proc. 3rd Asian Congress Fluid Mech., Tokyo, p. 331–334.

Sano, O. (1987), Steady thermal convection in a vertical torus, J. Phys. Soc. Jpn., **56**, 3893–3898.

Sano, O. (1988), Effect of asymmetry on the steady thermal convection in a vertical torus, J. Phys. Soc. Jpn., **57**, 1662–1668.

Sano, O. (1989), Chaotic behaviour of thermal convection in a vertical torus, Proc. 4th Asian Congress Fluid Mech., Hong-Kong, H37–H40.

Sano, O. (1991a), Cellular structure in natural convection loop and its chaotic behaviour. I. Experiment, Fluid Dynamics Research, **8**, 189–204.

Sano, O. (1991b), Cellular structure in natural convection loop and its chaotic behaviour. II. Theory, Fluid Dynamics Research, **8**, 205–220.

Sano, O. and Wakayama, T. (1989), An experimental study of the thermal convection in a vertical torus, J. Phys. Soc. Jpn., **58**, 2615–2618.

Segel, L. A. and Stuart, J. T. (1962), On the question of the preferred mode in cellular thermal convection, J. Fluid Mech., **13**, 289–306.

Stern, C. and Greif, R. (1987), Measurements in a natural convection loop, Wärme- und Stoffübertragung, **21**, 277–282.

Stewart, R. W. (1969), The atmosphere and the ocean, Scientific American, **221**, 76–86.

Stork, K. and Müller, U. (1972), Convection in boxes: experiments, J. Fluid Mech., **54**, 599–611.

Suda, F. and Mimura, K. (1989), Temperature and velocity distribution in a circular natural convection loop, 26th National Heat Transfer Symp. Jpn., Vol. 3, 752–754 (in Japanese).

Thomson, J. (1881), On a changing tesselated structure in certain liquids, Proc. Glasgow Phil. Soc., **13**, 464–468.

Tippelskirch, H. von (1956), Über Konvektionszellen, insbesondere im flüssigen Schwefel, Beiträge Phys. Atmos., **20**, 30–54.

Tritton, D. J. (1977), *Physical Fluid Dynamics*, Van Nostrand Rheinhold Co. Ltd., New York.

Welander, P. (1967), On the oscillatory instability of a differentially heated fluid loop, J. Fluid Mech., **29**, 17–30.

Widmann, P. J., Gorman, M., and Robbins, K. A. (1989), Nonlinear dynamics of a convection loop:

Chaos in laminar and turbulent flows, Physica, **36D**, 157–166.

Winet, H. and Jahn, T. L. (1972), On the origin of bioconvective fluid instabilities in *Tetrahymena* culture systems. Biorheol., **9**, 87–94.

Yorke, J. A. and Yorke, E. D. (1981), Chaotic behaviour and fluid dynamics, *Hydrodynamic Stability and the Transition to Turbulence* (Springer, Berlin), Chap. 4.

Yorke, J. A., Yorke, E. D., and Mallet-Paret, J. (1987), Lorenz-like chaos in a partial differential equation for a heated fluid loop, Physica, **24D**, 279–291.